J Intell Robot Syst (2018) 90:201–216
DOI 10.1007/s10846-017-0662-y

Composite Hierarchical Anti-Disturbance Control of a Quadrotor UAV in the Presence of Matched and Mismatched Disturbances

Ahmed Aboudonia[1] · Ramy Rashad[1] · Ayman El-Badawy[1]

Received: 17 September 2016 / Accepted: 5 June 2017 / Published online: 20 September 2017

Abstract Quadrotor helicopter is an unstable system subject to matched and mismatched disturbances. To stabilize the quadrotor dynamics in the presence of these disturbances, the application of a composite hierarchical anti-disturbance controller, combining a sliding mode controller and a disturbance observer, is presented in this paper. The disturbance observer is used to attenuate the effect of constant and slow time-varying disturbances. Whereas, the sliding mode controller is used to attenuate the effect of fast time-varying disturbances. In addition, sliding mode control attenuates the effect of the disturbance observer estimation errors of the constant and slow time-varying disturbances. In this approach, the upper bounds of the disturbance observer estimation errors are required instead of the disturbances' upper bounds. The disturbance observer estimation errors are found to be bounded when the disturbance observer dynamics are asymptotically stable and the disturbance derivatives and initial disturbances are bounded. Moreover, due to the highly nonlinear nature of the quadrotor dynamics, the upper bounds of a part of the quadrotor states and disturbance estimates are required. The nonlinear terms in the rotational dynamics are considered as disturbances, part of which is mismatched. This assumption simplifies the control system design by dividing the quadrotor's model into a position subsystem and a heading subsystem, and designing a controller for each separately. The stability analysis of the closed loop system is carried out using Lyapunov stability arguments. The effectiveness of the developed control scheme is demonstrated in simulations by applying different sources of disturbances such as wind gusts and partial actuator failure.

Keywords Disturbance observer · Sliding mode control · Quadrotor · Von karman wind

1 Introduction

Inspite of their instability, there is an increasing attention to quadrotor helicopters due to their broad variety of civil and military applications. This fact motivates the control systems researchers to develop and test different controllers to stabilize the quadrotor dynamics. These controllers include linear controllers, that usually work satisfactorily close to the hovering condition, as well as nonlinear controllers, that usually work properly away from the equilibrium point. Among these nonlinear controllers are the sliding mode controllers.

Sliding mode control design is mainly divided into two parts. The first part is the selection of the sliding surface. This surface is designed in such a way that, once reached, a reduced order model is obtained, whose dynamics is stable. Whereas, the second part is concerned with the design of the control law that guarantees reaching the sliding surface in finite time. This control law comprises two terms. First, the equivalent control term ensures staying on the sliding surface after being reached in the absence of disturbances. Second, the discontinuous control term ensures reaching the sliding surface in the presence of disturbances. Thus, using this control law, the behavior of the system is divided into two phases; a reaching phase in which the state trajectories are driven toward the sliding surface and a sliding phase in which the state trajectories slide along

✉ Ayman El-Badawy
ayman.elbadawy@guc.edu.eg

[1] German University in Cairo, Cairo, Egypt

the sliding surface (for more details, see [1]). Sliding mode controllers have been widely used for quadrotor control due to their robustness against external disturbances and model uncertainties.

In [2], the quadrotor rotational dynamics are divided into three subsystems describing the roll, pitch and yaw dynamics respectively. A sliding mode controller is designed to stabilize each of these subsystems separately. In [3], in addition to stabilizing the attitude dynamics using sliding mode control, the position and altitude dynamics are stabilized using linear control theory. In [4], the quadrotor dynamics are divided into two fully-actuated subsystems representing the altitude dynamics and the heading dynamics as well as an underactuated subsystem representing the position dynamics. The heading and the position subsystems are stabilized using sliding mode control. Whereas, the altitude dynamics are stabilized using a rate-bounded PID controller. To divide the quadrotor model into several subsystems in the above literature, some nonlinear terms in the rotational dynamics are ignored.

In [5] and [6], a sliding mode controller is developed based on the backstepping technique to stabilize the quadrotor dynamics. In [7], sliding mode control is used as a part of a fault tolerant controller to stabilize the quadrotor altitude and rotational dynamics in the presence of external disturbances and actuator faults. In [8], an integral sliding mode controller is developed to control the quadrotor altitude outdoors in and above ground effect. In [9], an adaptive sliding mode controller is developed based on the idea of input augmentation to get over the underactuation characteristics of the quadrotor. In [10], an adaptive sliding mode controller is designed to stabilize the quadrotor dynamics without the requirement of a priori known bound of the uncertainties. In [11], the quadrotor position and attitude tracking problem is solved using a second-order sliding mode controller. In all of the previously mentioned studies, external disturbances are either ignored in the analysis or handled using passive anti-disturbance control methods such as integral sliding mode control.

Recently, disturbance observer-based control and composite hierarchical anti-disturbance control ([12–14] and the references therein) have become well-known active anti-disturbance techniques used to attenuate the effect of matched and mismatched disturbances. Matched disturbances are the disturbances that affect the plant through the same channels of the inputs. On the other side, mismatched disturbances are those that influence the plant through channels different from those of the inputs. Disturbance observer-based control attenuates the effect of disturbances by relying on the disturbance estimates given by the disturbance observer. Composite hierarchical anti-disturbance control combines the disturbance observer with robust feedback controllers in such a way that the disturbance observer estimates are used to attenuate one part of the disturbances and the robust feedback controller is used to attenuate the other part. Thus, various disturbance observers are utilized within the quadrotor control systems in the literature.

In [15], the quadrotor dynamics are divided into six subsystems. In each subsystem, a linear frequency domain disturbance observer is integrated with a proportional-derivative controller to stabilize the quadrotor dynamics in the presence of wind gusts generated using a Dryden wind model. In [16], a linear state-space disturbance observer is augmented with a feedback linearization-based controller to stabilize the quadrotor dynamics in the case of partial actuator failure as well as in windy environments. In [17] and [18], a robust controller is developed by integrating a sliding mode disturbance observer with a sliding mode controller. To implement this control approach, the upper bounds of the disturbances affecting the quadrotor are required. In [19], a nonlinear disturbance observer augmented with a sliding mode controller is used to stabilize the quadrotor attitude dynamics only. The disturbances are assumed to be matched and slowly time-varying. In [20] and [21], sliding mode control is augmented with disturbance estimators as well in which the matching condition is also assumed.

As mentioned in [20] and [21], the matched disturbance assumption is standard in most of the literature of sliding mode control. Recently, a sliding mode controller is proposed in [22] in which the effect of mismatched disturbances is attenuated by combining this controller with a disturbance observer whose estimates are utilized in the design of the sliding surface and the control law. This composite controller requires only the upper bounds of the disturbance observer estimation errors. In [22], the developed controller is applied in simulation to a third-order single-input-single-output linear MAGLEV system.

The main aim of this paper is to apply a composite hierarchical anti-disturbance controller, that combines a sliding mode controller and a nonlinear disturbance observer, to stabilize the quadrotor's rotational and translational dynamics, which are multiple-input-multiple-output highly nonlinear, in the presence of both; matched and mismatched disturbances. The role of the disturbance observer is to estimate the values of constant and slow time-varying disturbances, whether they are matched or mismatched. Whereas the aim of the sliding mode controller is to cancel the effect of fast time-varying matched disturbances and the effect of the matched disturbance estimation errors. Moreover, the sliding mode controller attenuates the effect of the fast time-varying mismatched disturbances and the effect of the mismatched disturbance estimation errors. The disturbance estimates are used within the control system design based on the concept proposed in [22]. Thus, the developed disturbance observer-based sliding mode controller requires the upper bounds of the disturbance estimation errors instead

of the upper bounds of the disturbances themselves. However, due to the highly nonlinear nature of the quadrotor model, the upper bounds of a part of the quadrotor states and disturbance estimates are required as well.

The controller design is simplified by considering the nonlinear terms in the rotational dynamics as disturbances to be estimated using the disturbance observer. This assumption leads to the division of the controller into two parts; one for the heading control with a one-dimensional sliding surface and the other for the position control with three three-dimensional sliding surfaces. The effectiveness of the developed controller is investigated in simulations by implementing it on a quadrotor model in the presence of wind and partial actuator failure. Finally, it is worth mentioning that the matched disturbances include disturbing moments due to partial actuator failure and neglected gyroscopic effects in the rotational dynamics. While the mismatched disturbances include wind disturbances, disturbing forces due to partial actuator failure, and the nonlinear terms in the rotational kinematics.

The paper is organized as follows; the equations of motion of the quadrotor including the different sources of disturbances are presented in Section 2. Then, the disturbance observer-based sliding mode controller is developed in Section 3. In Section 4, the simulation results are introduced and discussed followed by the conclusion in the last section.

2 Dynamic Model

2.1 Quadrotor Nonlinear Model

The quadrotor dynamic model has been explored several times in the literature [23, 24]. The quadrotor is an underactuated multiple-input-multiple-output (MIMO) highly-nonlinear system with 6 degrees-of-freedom (DOFs) and 4 control inputs. The 6 DOFs represent the quadrotor position $\mathbf{P} = (x\ y\ z)^\top$ and attitude $\mathbf{\Theta} = (\phi\ \theta\ \psi)^\top$. The control inputs are the collective thrust force U_1, the rolling moment U_2, the pitching moment U_3 and the yawing moment U_4. The collective thrust force U_1 varies proportionally with the sum of squares of the angular speeds of the quadrotor's propellers. The rolling moment U_2 is generated due to the difference in the angular speeds of the left and right rotors. The pitching moment U_3 is generated due to the difference in the angular speeds of the front and rear rotors. The yawing moment U_4 varies proportionally with the difference between the sum of squares of the left and right rotors' angular speeds on one side and those of the front and rear rotors' angular speeds on the other side. In this subsection, the quadrotor kinematic relations and dynamic model are presented.

2.1.1 Quadrotor Kinematics

To derive the quadrotor kinematics, two reference frames are defined; the inertial frame fixed to the ground and the body-fixed reference frame attached to the center of mass of the quadrotor. Both reference frames are shown in Fig. 1. The rotation matrix $\mathbf{R}$ that transforms the axes of the body-fixed frame to the axes of the inertial frame is given by

$$\mathbf{R} = \begin{bmatrix} c_\theta c_\psi & s_\phi s_\theta c_\psi - c_\phi s_\psi & c_\phi s_\theta c_\psi + s_\phi s_\psi \\ c_\theta s_\psi & s_\phi s_\theta s_\psi + c_\phi c_\psi & c_\phi s_\theta s_\psi - s_\phi c_\psi \\ s_\theta & s_\phi c_\theta & c_\phi c_\theta \end{bmatrix}. \tag{1}$$

where ϕ is the roll angle, θ is the pitch angle, ψ is the yaw angle, $s_{(\cdot)}$ denotes the sine function and $c_{(\cdot)}$ denotes the cosine function. Moreover, the angular rate vector $\dot{\Theta} = [\dot\phi\ \dot\theta\ \dot\psi]^\top$ is related to the rotational velocity vector $\Omega = [p\ q\ r]^\top$ as follows

$$\begin{bmatrix} \dot\phi \\ \dot\theta \\ \dot\psi \end{bmatrix} = \begin{bmatrix} 1 & s_\phi t_\theta & c_\phi t_\theta \\ 0 & c_\phi & -s_\phi \\ 0 & s_\phi/c_\theta & c_\phi/c_\theta \end{bmatrix} \begin{bmatrix} p \\ q \\ r \end{bmatrix}. \tag{2}$$

where $t_{(\cdot)}$ represents the tangent function. By linearizing Eq. 2, the linearized equations are found to be

$$\dot\phi = p, \quad \dot\theta = q, \quad \dot\psi = r. \tag{3}$$

By considering the higher-order terms as disturbances denoted as d_ϕ, d_θ, d_ψ, the nonlinear relation in Eq. 2 can be expressed as

$$\begin{bmatrix} \dot\phi \\ \dot\theta \\ \dot\psi \end{bmatrix} = \begin{bmatrix} p + d_\phi \\ q + d_\theta \\ r + d_\psi \end{bmatrix}. \tag{4}$$

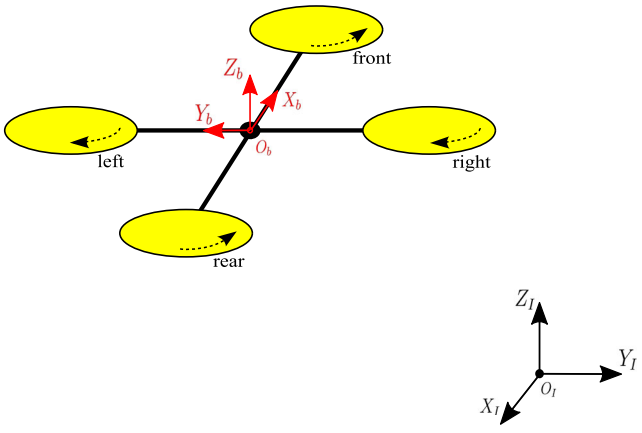

Fig. 1 Inertial and body-fixed reference frames

2.1.2 Quadrotor Dynamics

According to the Newton-Euler formalism, the quadrotor dynamics are written as

$$\begin{aligned} m\ddot{\mathbf{P}} &= \mathbf{F}, \\ \mathbf{I}\dot{\Omega} &= -\Omega \times \mathbf{I}\Omega + \mathbf{M}, \end{aligned} \tag{5}$$

where m is the quadrotor mass, $\mathbf{F}$ is the total force vector, $\mathbf{I} = diag\{I_x, I_y, I_z\}$ is the quadrotor inertia matrix and $\mathbf{M}$ is the total torque vector. Three main forces contribute to the total force affecting the quadrotor. These are the thrust force, the graviational force and the disturbing force. Therefore, the total force vector is expressed as

$$\mathbf{F} = \mathbf{RT} - m\mathbf{G} + \mathbf{D}_f, \tag{6}$$

where g is the gravitational acceleration, $\mathbf{G} = [0\ 0\ g]^\top$, $\mathbf{T} = [0\,0\,U_1]^\top$ and $\mathbf{D}_f = [d_x\ d_y\ d_z]^\top$ is the disturbing force vector. The thrust force U_1 and gravitational force mg occur in the third element of the vectors $\mathbf{T}$ and $m\mathbf{G}$ respectively because these two forces are applied along the Z_B and Z_I axes respectively. To represent the thrust force in the inertial reference frame, this force is multiplied by the rotation matrix $\mathbf{R}$. The disturbing force is assumed to be expressed in the inertial frame. There are two main torques contributing to the total torque influencing the quadrotor. These torques are the torques applied by the propellers $\mathbf{U}_m = [U_2\ U_3\ U_4]^\top$ and the disturbing torques $\mathbf{D}_m = [d_{up}\ d_{uq}\ d_{ur}]$. Thus, the total torque vector is represented as

$$\mathbf{M} = \mathbf{U}_m + \mathbf{D}_m. \tag{7}$$

Therefore, the quadrotor translational and rotational dynamics are expressed in detailed form, respectively, as

$$\begin{bmatrix} \ddot{x} \\ \ddot{y} \\ \ddot{z} \end{bmatrix} = \begin{bmatrix} (s_\phi s_\psi + c_\phi s_\theta c_\psi)\frac{U_1}{m} + \frac{d_x}{m} \\ (-s_\phi c_\psi + c_\phi s_\theta s_\psi)\frac{U_1}{m} + \frac{d_y}{m} \\ c_\phi c_\theta \frac{U_1}{m} - g + \frac{d_z}{m} \end{bmatrix}, \tag{8}$$

$$\begin{bmatrix} \dot{p} \\ \dot{q} \\ \dot{r} \end{bmatrix} = \begin{bmatrix} \frac{1}{I_x}[(I_y - I_z)qr + U_2 + d_{up}] \\ \frac{1}{I_y}[(I_z - I_x)pr + U_3 + d_{uq}] \\ \frac{1}{I_z}[(I_x - I_y)pq + U_4 + d_{ur}] \end{bmatrix}. \tag{9}$$

The disturbing force d_j along the axis $j \in \{x, y, z\}$ can be divided into a disturbing force due to wind d_{wj} and a disturbing force due to actuator failure d_{uj} as follows

$$\begin{bmatrix} d_x \\ d_y \\ d_z \end{bmatrix} = \begin{bmatrix} d_{wx} + d_{ux} \\ d_{wy} + d_{uy} \\ d_{wz} + d_{uz} \end{bmatrix}. \tag{10}$$

Similarly, the disturbing moment d_k, $k \in \{p, q, r\}$, can be divided into a disturbing moment due to ignored nonlinear dynamics d_{nk} and a disturbing moment due to actuator failure d_{uk} as follows

$$\begin{bmatrix} d_p \\ d_q \\ d_r \end{bmatrix} = \begin{bmatrix} d_{np} + d_{up} \\ d_{nq} + d_{uq} \\ d_{nr} + d_{ur} \end{bmatrix}. \tag{11}$$

The ignored nonlinear dynamics in Eq. 11 are considered to be

$$\begin{aligned} d_{np} &= (I_y - I_z)qr, \\ d_{nq} &= (I_z - I_x)pr, \\ d_{nr} &= (I_x - I_y)pq. \end{aligned} \tag{12}$$

The disturbing forces due to wind and the disturbing forces and moments due to partial actuator failure are discussed in the next subsections. The disturbing forces due to wind are considered to be applied to the center of mass of the quadrotor. Thus, the disturbing moments due to wind are considered negligible in this work.

2.2 State Space Model

A state space model of the quadrotor is presented in this subsection. The states of this model are chosen to be

$$\begin{aligned} \mathbf{x}_1 &= [x\ y\ z]^\top, \mathbf{x}_3 = [\phi\ \theta\ U_1]^\top, x_5 = \psi, \\ \mathbf{x}_2 &= [\dot{x}\ \dot{y}\ \dot{z}]^\top, \mathbf{x}_4 = \left[p\ q\ \dot{U}_1\right]^\top, x_6 = r, \end{aligned} \tag{13}$$

and its control inputs are selected to be

$$\mathbf{u}_1 = \left[\ddot{U}_1\ U_2\ U_3\right]^\top, u_2 = U_4. \tag{14}$$

In this case, the quadrotor nonlinear state space model is derived using Eqs. 4, 8, 9 and is written in the form

$$\dot{\mathbf{x}} = \mathbf{f}(\mathbf{x}, \mathbf{u}) + \mathbf{B_d}\mathbf{d}, \tag{15}$$

as follows

$$\begin{bmatrix} \dot{\mathbf{x}}_1 \\ \dot{\mathbf{x}}_2 \\ \dot{\mathbf{x}}_3 \\ \dot{\mathbf{x}}_4 \\ \dot{x}_5 \\ \dot{x}_6 \end{bmatrix} = \begin{bmatrix} \mathbf{x}_2 \\ \mathbf{f}_1(\mathbf{x}_3, \mathbf{x}_5) \\ \mathbf{x}_4 \\ \mathbf{J}_a\mathbf{u}_1 \\ x_6 \\ J_b u_2 \end{bmatrix} + \begin{bmatrix} 0_{3\times3} & 0_{3\times2} & 0_{3\times2} & 0_{3\times1} & 0_{3\times1} \\ \frac{1}{m}\mathbf{I}_{3\times3} & 0_{3\times2} & 0_{3\times2} & 0_{3\times1} & 0_{3\times1} \\ 0_{3\times3} & \mathbf{B}_{d2} & 0_{3\times2} & 0_{3\times1} & 0_{3\times1} \\ 0_{3\times3} & 0_{3\times2} & \mathbf{B}_{d3} & 0_{3\times1} & 0_{3\times1} \\ 0_{1\times3} & 0_{1\times2} & 0_{1\times2} & 1 & 0 \\ 0_{1\times3} & 0_{1\times2} & 0_{1\times2} & 0 & J_b \end{bmatrix} \begin{bmatrix} \mathbf{d}_1 \\ \mathbf{d}_2 \\ \mathbf{d}_3 \\ d_4 \\ d_5 \end{bmatrix}, \tag{16}$$

where

$$\mathbf{f}_1 = \begin{bmatrix} (s_\phi s_\psi + c_\phi s_\theta c_\psi)\frac{U_1}{m} \\ (-s_\phi c_\psi + c_\phi s_\theta s_\psi)\frac{U_1}{m} \\ c_\phi c_\theta \frac{U_1}{m} - g \end{bmatrix}, \mathbf{J}_a = \begin{bmatrix} 0 & \frac{1}{I_x} & 0 \\ 0 & 0 & \frac{1}{I_y} \\ 1 & 0 & 0 \end{bmatrix}, J_b = \frac{1}{I_z}, \mathbf{B}_{d2} = \begin{bmatrix} 1 & 0 \\ 0 & 1 \\ 0 & 0 \end{bmatrix}, \mathbf{B}_{d3} = \begin{bmatrix} \frac{1}{I_x} & 0 \\ 0 & \frac{1}{I_y} \\ 0 & 0 \end{bmatrix}. \quad (17)$$

According to the above state-space model, the disturbances affecting the quadrotor is found to be

$$\mathbf{d}_1 = \begin{bmatrix} d_x \\ d_y \\ d_z \end{bmatrix}, \mathbf{d}_2 = \begin{bmatrix} d_\phi \\ d_\theta \end{bmatrix}, \mathbf{d}_3 = \begin{bmatrix} d_p \\ d_q \end{bmatrix}, d_4 = d_\psi, \quad d_5 = d_r. \quad (18)$$

The matched disturbances include the disturbing moments $\mathbf{d}_3$ and d_5. Whereas, the mismatched disturbances include the disturbing forces $\mathbf{d}_1$ and the disturbances $\mathbf{d}_2$ and d_4 due to the linearization of the Euler rates' equation as illustrated in Eqs. 2 and 4.

2.3 Wind Disturbance Model

The wind velocities v_{wx}, v_{wy} and v_{wz} along the inertial axes are generated due to the summation of two main contributions; the first contribution is due to the mean wind velocities $\bar{v}_{wx}$, $\bar{v}_{wy}$ and $\bar{v}_{wz}$ produced by the discrete wind gust model [25] and [26] and the second one is due to the deviations from the mean wind velocities $\hat{v}_{wx}$, $\hat{v}_{wy}$ and $\hat{v}_{wz}$ produced by the simplified Von-Karman wind turbulence model [26]. This wind model follows the model discussed in [16] except that the Dryden wind model is replaced by the von karman wind model.

The velocity of the discrete wind gust model changes its value according to a 1-minus-cosine function as follows,

$$\bar{v}_{wj} = \begin{cases} \bar{v}_{wj1}, & 0 < t < t_1 \\ \bar{v}_{wj1} + \frac{(\bar{v}_{wj2} - \bar{v}_{wj1})}{2}\left(1 - \cos\left(\frac{\pi(t-t_1)}{t_2 - t_1}\right)\right), & t_1 < t < t_2 \\ \bar{v}_{wj2}, & t_2 < t \end{cases}, \quad (19)$$

where $\bar{v}_{wj1}$ and $\bar{v}_{wj2}$ are the wind velocities along the j axis before and after the wind gust respectively and t_1 and t_2 are the time instant at which the wind gust starts and stops respectively.

The velocity of the Von-Karman wind is generated by propagating band-limited white noise through the following filters

$$G_u(s) = \sigma_u \sqrt{\frac{2L_u}{\pi V}} \frac{1 + 0.25\frac{L_u}{V}s}{1 + 1.357\frac{L_u}{V}s + 0.1987\left(\frac{L_u}{V}\right)^2 s^2},$$

$$G_v(s) = \sigma_v \sqrt{\frac{L_v}{\pi V}} \frac{1 + 2.7478\frac{L_v}{V}s + 0.3398\left(\frac{L_v}{V}\right)^2 s^2}{1 + 2.9958\frac{L_v}{V}s + 1.9754\left(\frac{L_v}{V}\right)^2 s^2 + 0.1539\left(\frac{L_v}{V}\right)^3 s^3},$$

$$G_w(s) = \sigma_w \sqrt{\frac{L_w}{\pi V}} \frac{1 + 2.7478\frac{L_w}{V}s + 0.3398\left(\frac{L_w}{V}\right)^2 s^2}{1 + 2.9958\frac{L_w}{V}s + 1.9754\left(\frac{L_w}{V}\right)^2 s^2 + 0.1539\left(\frac{L_w}{V}\right)^3 s^3}, \quad (20)$$

where s is the *Laplace* variable, V is the quadrotor speed, the variables L_u, L_v and L_w are the turbulence scale lengths given by

$$L_w = z, \quad L_u = L_v = \frac{z}{(0.177 + 0.000823z)^{1.2}}, \quad (21)$$

the variables σ_u, σ_v and σ_w are the turbulence intensities given by

$$\sigma_w = 0.1W_{20}, \quad \sigma_u = \sigma_v = \frac{\sigma_w}{(0.177 + 0.000823z)^{0.4}}, \quad (22)$$

and W_{20} is the wind speed at a height of 6m.

Finally, the generated wind contributes to the drag force d_w applied to the quadrotor. The drag force components d_{wj} affecting the quadrotor in the presence of wind along the inertial axes $j \in \{x, y, z\}$ are expressed as,

$$d_{wj} = -\frac{1}{2}\rho C_{dj} A_j (v_j - v_{wj})^2 sgn(v_j - v_{wj}), \quad (23)$$

where ρ is the air density, C_{dj} is the quadrotor drag coefficient along the inertial axis j, A_j is the quadrotor projected area in a plane perpendicular to the inertial axis j and $sgn(\cdot)$ denotes the sign function. The terms v_j and v_{wj} are the quadrotor and wind velocities, respectively, along the inertial axes with respect to the ground. The areas A_x, A_y and A_z are computed as follows,

$$\mathbf{A_i} = \bar{\mathbf{R}}\mathbf{A_b}, \quad (24)$$

where $\mathbf{A_i} = [A_x\ A_y\ A_z]^T$ is a vector including the quadrotor projected areas in the planes perpendicular to the inertial axes, $\mathbf{A_b} = [A_u\ A_v\ A_w]^T$ is a vector including the quadrotor projected areas in the planes perpendicular to the body-fixed axes and $\bar{\mathbf{R}}$ is a matrix comprising the absolute values of the rotation matrix elements represented as

$$\bar{\mathbf{R}} = \begin{bmatrix} |c_\theta c_\psi| & |s_\phi s_\theta c_\psi - c_\phi s_\psi| & |c_\phi s_\theta c_\psi + s_\phi s_\psi| \\ |c_\theta s_\psi| & |s_\phi s_\theta s_\psi + c_\phi c_\psi| & |c_\phi s_\theta s_\psi - s_\phi c_\psi| \\ |s_\theta| & |s_\phi c_\theta| & |c_\phi c_\theta| \end{bmatrix}. \quad (25)$$

2.4 Actuator Failure Uncertainties

Partial actuator failure is carried out by supposing that the thrust force of the failed propeller, at a certain speed, reaches a value lower than the expected one. Although the developed

controller is independent of which rotor fails, we consider, in this work, the case of the front propeller failure in which the actual control input vector $\bar{\mathbf{U}}$ is related to the computed control input vector $\mathbf{U}$ as follows

$$\bar{\mathbf{U}} = \Lambda \mathbf{U}, \tag{26}$$

such that

$$\Lambda = \begin{bmatrix} \frac{3+\lambda}{4} & 0 & \frac{1-\lambda}{2l_a} & \frac{b-b\lambda}{4d} \\ 0 & 1 & 0 & 0 \\ \frac{l_a-l_a\lambda}{4} & 0 & \frac{1+\lambda}{2} & \frac{bl_a(-1+\lambda)}{4d} \\ \frac{d-d\lambda}{4b} & 0 & \frac{d(-1+\lambda)}{2bl_a} & \frac{3+\lambda}{4} \end{bmatrix}. \tag{27}$$

where l_a is the distance between the center of the quadrotor and the axis of rotation of the front rotor, b is the thrust coefficient, d is the drag coefficient and λ is the front rotor's degree of effectiveness. The relation in Eqs. 26, 27 is derived in details in [16]. If partial actuator failure exists, the disturbing forces along the axes of the inertial frames are found to be

$$\begin{aligned} d_{ux} &= (s_\phi s_\psi + c_\phi s_\theta c_\psi) d_{u1}, \\ d_{uy} &= (-s_\phi c_\psi + c_\phi s_\theta s_\psi) d_{u1}, \\ d_{uz} &= (c_\phi c_\theta) d_{u1}. \end{aligned} \tag{28}$$

where $d_{u1} = \bar{U}_1 - U_1$ expresses the disturbing force along the body-fixed Z_B axis. Whereas, the disturbing moments are

$$\begin{aligned} d_{up} &= \bar{U}_2 - U_2, \\ d_{uq} &= \bar{U}_3 - U_3, \\ d_{ur} &= \bar{U}_4 - U_4. \end{aligned} \tag{29}$$

3 Control System Design

In this section, the controller design is presented in two steps. First, a disturbance observer is designed for disturbance estimation. Then, a sliding mode controller is designed to stabilize the quadrotor dynamics using the disturbance estimates.

3.1 Disturbance Observer

The aim of the disturbance observer is to estimate the disturbances affecting the quadrotor so that these estimates can be used, afterwards, within the control law to attenuate the effect of the actual disturbances. The disturbance observer [12] used in this work is given by

$$\begin{aligned} \dot{\mathbf{z}} &= -\mathbf{L}\mathbf{B_d}\mathbf{z} - \mathbf{L}(\mathbf{f}(\mathbf{x}, \mathbf{u}) + \mathbf{B_d}\mathbf{L}\mathbf{x}), \\ \hat{\mathbf{d}} &= \mathbf{z} + \mathbf{L}\mathbf{x}. \end{aligned} \tag{30}$$

where $\hat{\mathbf{d}}$ is the disturbance estimate vector, $\mathbf{z}$ is the disturbance observer internal state vector and $\mathbf{L}$ is the disturbance observer gain matrix. By defining the disturbance observer error $\mathbf{e_d}$ to be the error between the actual disturbances and the estimated ones, then, the disturbance observer error dynamics is found to be

$$\dot{\mathbf{e}}_\mathbf{d} = -\mathbf{L}\mathbf{B_d}\mathbf{e_d} + \dot{\mathbf{d}}. \tag{31}$$

Hence, the gain matrix $\mathbf{L}$ is selected such that the matrix $\mathbf{LB_d}$ has eigenvalues with positive real parts to stabilize the error dynamics. To keep the disturbance observer error dynamics decoupled, the gain matrix $\mathbf{L}$ is selected to be

$$\mathbf{L} = \mathbf{L_d}\mathbf{B_d}^+, \tag{32}$$

where $\mathbf{B}_d^+$ is the pseudo-inverse of the matrix $\mathbf{B}_d$ and $\mathbf{L_d} = diag(\mathbf{L}_{d1}, ..., L_{d5})$ is a positive definite diagonal matrix with $\mathbf{L}_{d1} = l_{d1}\mathbf{I}_{3\times3}$, $\mathbf{L}_{d2} = l_{d2}\mathbf{I}_{2\times2}$, $\mathbf{L}_{d3} = l_{d3}\mathbf{I}_{2\times2}$, $L_{d4} = l_{d4}$ and $L_{d5} = l_{d5}$. Therefore, the error dynamics are represented as

$$\dot{\mathbf{e}}_\mathbf{d} = -\mathbf{L_d}\mathbf{e_d} + \dot{\mathbf{d}}. \tag{33}$$

The disturbance observer error dynamics in Eq. 33 represent a first-order high-pass filter between each disturbance observer estimation error and the corresponding disturbance. Therefore, it can be inferred that, although this observer is designed to estimate constant disturbances, it can also provide satisfactory estimates for the disturbances with frequencies below its bandwidth determined by $\mathbf{L}_d$. Thus, in general, this disturbance observer can estimate constant and slow time-varying disturbances. As for relatively fast time-varying disturbances, the disturbance observer estimation error is approximately equal in magnitude to the disturbance itself. In this case, the effect of such disturbances is attenuated using the sliding mode controller as shown in the next subsections. The solution of the system represented by the set of the first-order linear differential equations in Eq. 33 is found to be

$$\mathbf{e_d}(t) = e^{-\mathbf{L}_d t}\mathbf{e_d}(0) + \int_0^t e^{-\mathbf{L}_d(t-\tau)}\dot{\mathbf{d}}(\tau)d\tau \tag{34}$$

where t is the time variable and e is the Euler's number. As indicated in [27], since the dynamics in Eq. 33 is asymptotically stable, then, for each ϵ_j, $j \in \{x, y, z, \phi, \theta, \psi, p, q, r\}$, there exist δ_j and k_j such that

$$e_{dj}(0) < \delta_j \text{ and } \dot{d}_j(t) < k_j \text{ imply } e_{dj}(t) < \epsilon_j, \quad \forall t \geq 0. \tag{35}$$

By choosing the initial values of the disturbance observer's estimates to be zero, the conditions in Eq. 35 are modified to be

$$d_j(0) < \delta_j \text{ and } \dot{d}_j(t) < k_j \text{ imply } e_{dj}(t) < \epsilon_j, \quad \forall t \geq 0. \tag{36}$$

Thus, these conditions guarantee the boundedness of the disturbance observer estimation errors. Notice also that,

since $\dot{\mathbf{e}}_\mathbf{d} = \dot{\mathbf{d}} - \dot{\hat{\mathbf{d}}}$, the error dynamics in Eq. 33 can be written as

$$\dot{\hat{\mathbf{d}}} = \mathbf{L_d e_d}. \tag{37}$$

This relation will be used later in the sliding mode controller design.

3.2 Sliding Mode Controller Design

In this subsection, a sliding mode controller is designed to stabilize the quadrotor dynamics in the presence of disturbances. To design the sliding mode controller, the quadrotor model is divided into two subsystems. The first subsystem describes the position dynamics and includes the states $\mathbf{x}_1$, $\mathbf{x}_2$, $\mathbf{x}_3$ and $\mathbf{x}_4$. While the second subsystem describes the heading dynamics and includes the states x_5 and x_6.

3.2.1 Heading Controller Design

The heading sliding mode controller is designed in this subsection. Similar to [22], the sliding surface S_h of this subsystem is designed to be

$$S_h = c_h e_{h1} + e_{h2} + \hat{d}_4, \tag{38}$$

where

$$\begin{aligned} e_{h1} &= x_5 - x_{5d}, \\ e_{h2} &= x_6 - \dot{x}_{5d}, \end{aligned} \tag{39}$$

where c_h is a controller gain to be chosen later, x_{5d} is the desired heading trajectory, $\hat{d}_4$ is the disturbance estimate of the disturbance d_4 obtained by the disturbance observer. Using Eqs. 16, 37, the derivative of the heading subsystem sliding surface is found to be

$$\dot{S}_h = c_h(x_6 + d_4 - \dot{x}_{5d}) + (J_b u_2 + J_b d_5 - \ddot{x}_{5d}) + l_{d4} e_{d4}, \tag{40}$$

where e_{d4} is the disturbance observer estimation error of the disturbance d_4. Let the Lyapunov function of the heading subsystem sliding surface be

$$V_h = \frac{1}{2} S_h^2. \tag{41}$$

Thus, the derivative of the Lyapunov function is found to be

$$\begin{aligned} \dot{V}_h = S_h \dot{S}_h = S_h \, [&c_h(x_6 + d_4 - \dot{x}_{5d}) + J_b u_2 \\ &+ J_b d_5 - \ddot{x}_{5d} + l_{d4} e_{d4}] \, . \end{aligned} \tag{42}$$

By designing the control input u_2 to be

$$\begin{aligned} u_2 = -J_b^{-1} \Big(&c_h(x_6 + \hat{d}_4 - \dot{x}_{5d}) + J_b \hat{d}_5 - \ddot{x}_{5d} \\ &+ k_{hs} sgn(S_h) + k_h S_h \Big) , \end{aligned} \tag{43}$$

where k_{hs} and k_h are controller gains to be chosen later, the derivative of the Lyapunov function is modified to be

$$\dot{V}_h = S_h \, [(c_h + l_{d4}) e_{d4} + J_2 \mathbf{e}_{d5}] - k_{hs} |S_h| - k_h S_h^2. \tag{44}$$

where e_{d5} is the disturbance observer estimation error of the disturbance d_5. Denoting e_{d4+} and e_{d5+} as the upper bounds of e_{d4} and e_{d5}, the gains k_{hs} and k_h can be chosen as follows,

$$\begin{aligned} k_{hs} &> (c_h + l_{d4}) e_{d4+} + J_b e_{d5+}, \\ k_h &> 0. \end{aligned} \tag{45}$$

In this case, the Lyapunov function derivative becomes negative definite guaranteeing the stability of the heading subsystem sliding surface dynamics. Recall that the disturbance observer estimation errors e_{d4} and e_{d5} include those of the fast time-varying disturbances that are poorly estimated by the disturbance observer. At $S_h = 0$, the error dynamics is found to be

$$\dot{e}_{h1} = -c_h e_{h1} + e_{d4}. \tag{46}$$

Thus, to stabilize the dynamics at $S_h = 0$, the gain c_h is selected to be $c_h > 0$. Therefore, the boundedness of e_{d4} guarantees the boundedness of e_{h1}.

3.2.2 Position Controller Design

In this subsection, the position sliding mode controller is designed. The three position sliding surfaces are selected to be

$$\mathbf{S}_p = c_1 \mathbf{e}_{p1} + c_2 \mathbf{e}_{p2} + c_3 \mathbf{e}_{p3} + \mathbf{e}_{p4}, \tag{47}$$

where

$$\begin{aligned} \mathbf{e}_{p1} &= \mathbf{x}_1 - \mathbf{x}_{1d}, \\ \mathbf{e}_{p2} &= \mathbf{x}_2 - \dot{\mathbf{x}}_{1d}, \\ \mathbf{e}_{p3} &= \mathbf{f}_1(\mathbf{x}_3, \mathbf{x}_5) + \frac{1}{m} \hat{\mathbf{d}}_1 - \ddot{\mathbf{x}}_{1d}, \\ \mathbf{e}_{p4} &= \mathbf{J}_h(\mathbf{x}_3, \mathbf{x}_5)[x_6 + \hat{d}_4] + \mathbf{J}_p(\mathbf{x}_3, \mathbf{x}_5)[\mathbf{x}_4 + \mathbf{B}_{d2} \hat{\mathbf{d}}_2] - \mathbf{x}_{1d}^{(3)}, \end{aligned} \tag{48}$$

and c_1, c_2 and c_3 are controller gains to be chosen later, $\mathbf{x}_{1d}$ is the desired position trajectory, $\hat{\mathbf{d}}_1$, $\hat{\mathbf{d}}_2$ and $\hat{d}_4$ are the disturbance estimates of the disturbances $\mathbf{d}_1$, $\mathbf{d}_2$ and d_4 respectively, $\mathbf{J}_h = \partial \mathbf{f}_1 / \partial x_5$ and $\mathbf{J}_p = \partial \mathbf{f}_1 / \partial \mathbf{x}_3$. Using Eqs.16, 37, the derivative of the position sliding surfaces is found to be

$$\begin{aligned} \dot{\mathbf{S}}_p = \; &c_1(\mathbf{x}_2 - \dot{\mathbf{x}}_{1d}) + c_2(\mathbf{f}_1 + \frac{1}{m} \mathbf{d}_1 - \ddot{\mathbf{x}}_{1d}) \\ &+ c_3(\mathbf{J}_h[x_6 + d_4] + \mathbf{J}_p[\mathbf{x}_4 + \mathbf{B}_{d2} \mathbf{d}_2] + \frac{l_{d1}}{m} \mathbf{e}_{d1} - \mathbf{x}_{1d}^{(3)}) \end{aligned}$$

$$+\mathbf{J}_h[J_b u_2 + J_b d_5 + l_{d4} e_{d4}] + \mathbf{J}_p\,[\mathbf{J}_a \mathbf{u}_1 + \mathbf{B}_{d3}\mathbf{d}_3 + \mathbf{B}_{d2} l_{d2} \mathbf{e}_{d2}] + [\dot{\mathbf{J}}_p\ \dot{\mathbf{J}}_h]\left[\mathbf{x}_4 + \mathbf{B}_{d2}\hat{\mathbf{d}}_2 x_6 + \hat{d}_4\right] - \mathbf{x}_{1d}^{(4)}, \tag{49}$$

where $\mathbf{e}_{d1}$, $\mathbf{e}_{d2}$ and e_{d4} are the disturbance observer estimation errors of the disturbances $\mathbf{d}_1$, $\mathbf{d}_2$ and d_4 respectively and

$$\dot{\mathbf{J}}_p = \frac{\partial \mathbf{J}_p}{\partial \phi}(p + d_\phi) + \frac{\partial \mathbf{J}_p}{\partial \theta}(q + d_\theta) + \frac{\partial \mathbf{J}_p}{\partial \psi}(r + d_\psi) + \frac{\partial \mathbf{J}_p}{\partial U_1}\dot{U}_1,$$
$$\dot{\mathbf{J}}_h = \frac{\partial \mathbf{J}_h}{\partial \phi}(p + d_\phi) + \frac{\partial \mathbf{J}_h}{\partial \theta}(q + d_\theta) + \frac{\partial \mathbf{J}_h}{\partial \psi}(r + d_\psi) + \frac{\partial \mathbf{J}_h}{\partial U_1}\dot{U}_1. \tag{50}$$

Let the Lyapunov function of the position subsystem be defined as

$$V_p = \frac{1}{2}\mathbf{S}_p^\top \mathbf{S}_p. \tag{51}$$

The derivative of this Lyapunov function is found to be

$$\dot{V}_p = \mathbf{S}_p^\top \dot{\mathbf{S}}_p, \tag{52}$$

where $\dot{\mathbf{S}}_p$ is expressed as in Eq. 49. By substituting Eq. 50 in Eq. 49 and choosing the control input $\mathbf{u}_1$ to be

$$\begin{aligned}\mathbf{u}_1 = -(\mathbf{J}_p\mathbf{J}_a)^{-1}\Bigg(& c_1(\mathbf{x}_2 - \dot{\mathbf{x}}_{1d}) + c_2(\mathbf{f}_1 + \frac{1}{m}\hat{\mathbf{d}}_1 - \ddot{\mathbf{x}}_{1d}) \\ &+ c_3(\mathbf{J}_h[x_6 + \hat{d}_4] + \mathbf{J}_p[\mathbf{x}_4 + \mathbf{B}_{d2}\hat{\mathbf{d}}_2] - \mathbf{x}_{1d}^{(3)}) \\ &+ \mathbf{J}_h[J_b u_2 + J_b \hat{d}_5] + \mathbf{J}_p \mathbf{B}_{d3}\hat{\mathbf{d}}_3 \\ &+ \Bigg((p + \hat{d}_\phi)\begin{bmatrix}\frac{\partial \mathbf{J}_p}{\partial \phi} & \frac{\partial \mathbf{J}_h}{\partial \phi}\end{bmatrix} + (q + \hat{d}_\theta)\begin{bmatrix}\frac{\partial \mathbf{J}_p}{\partial \theta} & \frac{\partial \mathbf{J}_h}{\partial \theta}\end{bmatrix} \\ &+ (r + \hat{d}_\psi)\begin{bmatrix}\frac{\partial \mathbf{J}_p}{\partial \psi} & \frac{\partial \mathbf{J}_h}{\partial \psi}\end{bmatrix} + \dot{U}_1\begin{bmatrix}\frac{\partial \mathbf{J}_p}{\partial U_1} & \frac{\partial \mathbf{J}_h}{\partial U_1}\end{bmatrix}\Bigg)\left[\mathbf{x}_4 + \mathbf{B}_{d2}\hat{\mathbf{d}}_2 x_6 + \hat{d}_4\right] \\ &- \mathbf{x}_{1d}^{(4)} + k_{ps}\,sgn(\mathbf{S}_p) + k_p \mathbf{S}_p\Bigg),\end{aligned} \tag{53}$$

where k_{ps} and k_p are controller gains to be selected later and $\hat{\mathbf{d}}_3$ and $\hat{d}_5$ are the disturbance estimates of the disturbances $\mathbf{d}_3$ and d_5, the derivative of the Lyapunov function $\dot{V}_p$ is modified to be

$$\dot{V}_p = \mathbf{S}_p^\top \begin{pmatrix} \frac{1}{m}(c_2 + c_3 l_{d1})\mathbf{e}_{d1} + \mathbf{J}_p \mathbf{B}_{d2}(c_3 + l_{d2})\mathbf{e}_{d2} + \mathbf{J}_p \mathbf{B}_{d3}\mathbf{e}_{d3} \\ + \mathbf{J}_h(c_3 + l_{d4})e_{d4} + \mathbf{J}_h J_b e_{d5} - k_{ps}\,sgn(\mathbf{S}_p) - k_p \mathbf{S}_p \\ + \left(e_{d\phi}\begin{bmatrix}\frac{\partial \mathbf{J}_p}{\partial \phi} & \frac{\partial \mathbf{J}_h}{\partial \phi}\end{bmatrix} + e_{d\theta}\begin{bmatrix}\frac{\partial \mathbf{J}_p}{\partial \theta} & \frac{\partial \mathbf{J}_h}{\partial \theta}\end{bmatrix} + e_{d\psi}\begin{bmatrix}\frac{\partial \mathbf{J}_p}{\partial \psi} & \frac{\partial \mathbf{J}_h}{\partial \psi}\end{bmatrix}\right)\begin{bmatrix}\mathbf{x}_4 + \mathbf{B}_{d2}\hat{\mathbf{d}}_2 \\ x_6 + \hat{d}_4\end{bmatrix} \end{pmatrix}, \tag{54}$$

where $\mathbf{e}_{d3}$ and e_{d5} are the disturbance observer estimation errors of the disturbances $\mathbf{d}_3$ and d_5 respectively. The control signal u_2 can be used to compute the control signal $\mathbf{u}_1$ since u_2 is already computed earlier while designing the heading controller. The term $sgn(\mathbf{S}_p)$ gives a vector of the same size as $\mathbf{S}_p$ and whose elements are the signs of the corresponding elements in $\mathbf{S}_p$. The determinant of the matrix $\mathbf{J}_p\mathbf{J}_a$ is found to be

$$|\mathbf{J}_p\mathbf{J}_a| = \frac{U_1^2 c_\phi}{m^3 I_x I_y}. \tag{55}$$

Thus, the matrix $\mathbf{J}_p\mathbf{J}_a$ is always invertible as long as $U_1 \neq 0$ and $-\frac{\pi}{2} < \phi < \frac{\pi}{2}$ which are satisfied during the normal flight conditions. By defining $\mathbf{J}_u$ as the third column of the matrix $\mathbf{J}_p$, $\mathbf{J}_{ph} = [\mathbf{J}_p\mathbf{B}_{d2} \quad \mathbf{J}_h]$ and

$$\mathbf{e}_{ph} = \begin{bmatrix}(c_3 + l_{d2})\mathbf{e}_{d2} + \mathbf{B}_{d2}^+ \mathbf{B}_{d3}\mathbf{e}_{d3} \\ (c_3 + l_{d4})e_{d4} + J_b e_{d5}\end{bmatrix},$$
$$\mathbf{x}_e = \begin{bmatrix}\mathbf{B}_{d2}^+ \mathbf{x}_4 + \hat{\mathbf{d}}_2 \\ x_6 + \hat{d}_4\end{bmatrix} = \begin{bmatrix}p + \hat{d}_\phi \\ q + \hat{d}_\theta \\ r + \hat{d}_\psi\end{bmatrix}, \tag{56}$$

the Lyapunov function derivative Eq. 54 can be written as

$$\begin{aligned}\dot{V}_p =\ & \mathbf{S}_p^\top\Bigg[\frac{1}{m}(c_2 + c_3 l_{d1})\mathbf{e}_{d1} + \mathbf{J}_{ph}\mathbf{e}_{ph} + \left(e_{d\phi}\frac{\partial \mathbf{J}_{ph}}{\partial \phi} + e_{d\theta}\frac{\partial \mathbf{J}_{ph}}{\partial \theta} + e_{d\psi}\frac{\partial \mathbf{J}_{ph}}{\partial \psi}\right)\mathbf{x}_e \\ &+ \left(e_{d\phi}\frac{\partial \mathbf{J}_u}{\partial \phi} + e_{d\theta}\frac{\partial \mathbf{J}_u}{\partial \theta} + e_{d\psi}\frac{\partial \mathbf{J}_u}{\partial \psi}\right)\dot{U}_1 - k_{ps}\,sgn(\mathbf{S}_p) - k_p \mathbf{S}_p\Bigg].\end{aligned} \tag{57}$$

To ensure that the Lyapunov function derivative $\dot{V}_p$ is negative definite, the following conditions have to be satisfied

$$\begin{aligned}& k_p > 0, \\ & k_{ps}\sum_{i=1}^{3}|S_{pi}| > \sum_{i=1}^{3}\left(\begin{array}{c}\frac{1}{m}(c_2 + c_3 l_{d1})e_{d1i} + \mathbf{J}_{phi}\mathbf{e}_{ph} + \left(e_{d\phi}\frac{\partial \mathbf{J}_{phi}}{\partial \phi} + e_{d\theta}\frac{\partial \mathbf{J}_{phi}}{\partial \theta} + e_{d\psi}\frac{\partial \mathbf{J}_{phi}}{\partial \psi}\right)\mathbf{x}_e \\ + \left(e_{d\phi}\frac{\partial \mathbf{J}_{ui}}{\partial \phi} + e_{d\theta}\frac{\partial \mathbf{J}_{ui}}{\partial \theta} + e_{d\psi}\frac{\partial \mathbf{J}_{ui}}{\partial \psi}\right)\dot{U}_1\end{array}\right) S_{pi},\end{aligned} \tag{58}$$

where $e_{d11} = e_{dx}$, $e_{d12} = e_{dy}$ and $e_{d13} = e_{dz}$ are the components of the vector $\mathbf{e}_{d1}$ and S_{pi}, J_{phi} and J_{ui} are the ith rows of $\mathbf{S}_p$, $\mathbf{J}_{ph}$ and $\mathbf{J}_u$ respectively. By defining e_{dj+}, $j = \{x, y, z, \phi, \theta, \psi, p, q, r\}$ as the upper bounds of the absolute disturbance observer estimation errors $|e_{dj}|$, the following vectors can be defined

$$\mathbf{e}_{d1+} = \begin{bmatrix} e_{d11+} \\ e_{d12+} \\ e_{d13+} \end{bmatrix} = \begin{bmatrix} e_{dx+} \\ e_{dy+} \\ e_{dz+} \end{bmatrix}, \quad \mathbf{e}_{d2+} = \begin{bmatrix} e_{d\phi+} \\ e_{d\theta+} \end{bmatrix},$$
$$\mathbf{e}_{d3+} = \begin{bmatrix} e_{dp+} \\ e_{dq+} \end{bmatrix}, \quad e_{d4+} = e_{d\psi+}, \quad e_{d5+} = e_{dr+}, \quad (59)$$

and consequently,

$$\mathbf{e}_{ph+} = \begin{bmatrix} (c_3 + l_{d2})\mathbf{e}_{d2+} + \mathbf{B}_{d2}^{+}\mathbf{B}_{d3}\mathbf{e}_{d3+} \\ (c_3 + l_{d4})e_{d4+} + J_b e_{d5+} \end{bmatrix}. \quad (60)$$

In addition, let $\mathbf{x}_{e+}$, $\mathbf{J}_{phi+}$, $\partial\mathbf{J}_{phi}/\partial\phi_+$, $\partial\mathbf{J}_{phi}/\partial\theta_+$, $\partial\mathbf{J}_{phi}/\partial\psi_+$, $\partial\mathbf{J}_{ui}/\partial\phi_+$, $\partial\mathbf{J}_{ui}/\partial\theta_+$ and $\partial\mathbf{J}_{ui}/\partial\psi_+$ be vectors whose elements represent the upper bounds of the absolute values of the elements in the corresponding vectors. Moreover, let $|U_1| < U_{1+}$, $|\dot{U}_1| < \dot{U}_{1+}$ and denote $||(\cdot)||_\infty$ as the infinity norm of the corresponding matrix or vector. To satisfy the inequality in Eq. 58, the gain k_{ps} is selected to be

$$\begin{aligned} k_{ps} > \max_i \Bigg\{ & \frac{c_2 + c_3 l_{d1}}{m} e_{d1i+} + ||\mathbf{J}_{phi+}||_\infty ||\mathbf{e}_{ph+}||_\infty \\ & + \left(e_{d\phi+} || \frac{\partial \mathbf{J}_{phi}}{\partial \phi_+} ||_\infty + e_{d\theta+} || \frac{\partial \mathbf{J}_{phi}}{\partial \theta_+} ||_\infty + e_{d\psi+} || \frac{\partial \mathbf{J}_{phi}}{\partial \psi_+} ||_\infty \right) ||\mathbf{x}_{e+}||_\infty \\ & + \left(e_{d\phi+} || \frac{\partial \mathbf{J}_{ui}}{\partial \phi_+} ||_\infty + e_{d\theta+} || \frac{\partial \mathbf{J}_{ui}}{\partial \theta_+} ||_\infty + e_{d\psi+} || \frac{\partial \mathbf{J}_{ui}}{\partial \psi_+} ||_\infty \right) \dot{U}_{1+} \Bigg\}, \quad (61) \end{aligned}$$

guaranteeing the stability of the position surface dynamics. Recall that the disturbance observer estimation errors include those of the fast time-varying disturbances that are poorly estimated by the disturbance observer. Since $\mathbf{J}_{ph}$ and $\mathbf{J}_u$ are trigonometric functions of the Euler angles, the infinity norms of these matrices and their partial derivatives can be computed by investigating the whole range of operation of the euler angles; $-\pi/2 < \phi < \pi/2$, $\pi/2 < \theta < \pi/2$, $-\pi \leq \psi \leq \pi$. It is found that $||\mathbf{J}_{ph}||_\infty = ||\partial\mathbf{J}_{ph}/\partial\phi||_\infty = ||\partial\mathbf{J}_{ph}/\partial\psi||_\infty = 2.137U_{1+}/m$, $||\partial\mathbf{J}_{ph}/\partial\theta||_\infty = 1.1546U_{1+}/m$ and $||\partial\mathbf{J}_u/\partial\phi||_\infty = ||\partial\mathbf{J}_u/\partial\theta||_\infty = ||\partial\mathbf{J}_u/\partial\psi||_\infty = 1/m$. Thus, the inequality in Eq. 61 is guaranteed by choosing k_{ps} as follows

$$\begin{aligned} k_{ps} > & \frac{1}{m}(c_2 + c_3 l_{d1})||e_{d1+}||_\infty + 2.13U_{1+}||\mathbf{e}_{ph+}||_\infty/m \\ & + \left(2.13e_{d\phi+} + 1.14e_{d\theta+} + 2.13e_{d\psi+}\right) U_{1+}||\mathbf{x}_{e+}||_\infty/m \\ & + \left(e_{d\phi+} + e_{d\theta+} + e_{d\psi+}\right) \dot{U}_{1+}/m, \quad (62) \end{aligned}$$

Hence, the lower bound of the gain k_{ps} can be chosen based on the upper bounds of the closed loop quadrotor states and disturbance estimates; U_{1+}, $\dot{U}_{1+}$ and $\mathbf{x}_{e+}$ as well as the upper bounds of the disturbance observer estimation errors $\mathbf{e}_{d1+}$, $\mathbf{e}_{ph+}$, $e_{d\phi+}$, $e_{d\theta+}$ and $e_{d\psi+}$ which are proven to be bounded under the conditions in Eq. 36. At $S_p = 0$, the position error dynamics is found to be

$$\begin{aligned} \begin{bmatrix} \dot{\mathbf{e}}_{p1} \\ \dot{\mathbf{e}}_{p2} \\ \dot{\mathbf{e}}_{p3} \end{bmatrix} = & \begin{bmatrix} 0_{3\times3} & \mathbf{I}_{3\times3} & 0_{3\times3} \\ 0_{3\times3} & 0_{3\times3} & \mathbf{I}_{3\times3} \\ -c_1\mathbf{I}_{3\times3} & -c_2\mathbf{I}_{3\times3} & -c_3\mathbf{I}_{3\times3} \end{bmatrix} \begin{bmatrix} \mathbf{e}_{p1} \\ \mathbf{e}_{p2} \\ \mathbf{e}_{p3} \end{bmatrix} \\ & + \begin{bmatrix} 0_{3\times3} & 0_{3\times2} & 0_{3\times1} \\ \mathbf{I}_{3\times3}/m & 0_{3\times2} & 0_{3\times1} \\ \mathbf{L}_{d1}/m & \mathbf{J}_p\mathbf{B}_{d2} & \mathbf{J}_h \end{bmatrix} \begin{bmatrix} \mathbf{e}_{d1} \\ \mathbf{e}_{d2} \\ e_{d4} \end{bmatrix}. \quad (63) \end{aligned}$$

Thus, to stabilize the dynamics at $S_p = 0$ in the absence of disturbances, the gains c_1, c_2 and c_3 are selected such that the polynomial $p(s) = s^3 + c_3 s^2 + c_2 s + c_1$ is Hurwitz where s is the Laplace variable.

3.3 Composite Error Dynamics

As long as the sliding mode controller gains k_{hs} and k_{ps} are chosen as in Eqs. 45 and 62, the sliding surfaces S_h and $\mathbf{S}_p$ are reached. Notice that, on the sliding surface $\mathbf{S}_p$, the reduced-order model in Eq. 63 is nonlinear due to the existence of the matrices $\mathbf{J}_p$ and $\mathbf{J}_h$ that are functions of the quadrotor states. By linearizing the reduced order model in Eq. 63 around $(\mathbf{e}_p^\top, e_h, \mathbf{e}_d^\top) = (\mathbf{e}_{p,o}^\top, e_{h,o}, \mathbf{0}_{1\times9})$ and, then, combining the linearized model with the dynamics in Eqs. 33, 46, the linearized combined error dynamics of the whole system on the sliding surfaces can be written as

$$\begin{bmatrix} \dot{\mathbf{e}} \\ \dot{\mathbf{e}}_d \end{bmatrix} = \begin{bmatrix} \mathbf{A} & \mathbf{B} \\ \mathbf{0}_{5\times4} & -\mathbf{L}_d \end{bmatrix} \begin{bmatrix} \mathbf{e} \\ \mathbf{e}_d \end{bmatrix} + \begin{bmatrix} \mathbf{0}_{4\times5} \\ \mathbf{I}_{5\times5} \end{bmatrix} \dot{\mathbf{d}}_p \quad (64)$$

where

$$\mathbf{e} = \begin{bmatrix} \mathbf{e}_{p1} \\ \mathbf{e}_{p2} \\ \mathbf{e}_{p3} \\ e_h \end{bmatrix}, \quad \mathbf{A} = \begin{bmatrix} 0_{3\times3} & \mathbf{I}_{3\times3} & 0_{3\times3} & 0_{3\times1} \\ 0_{3\times3} & 0_{3\times3} & \mathbf{I}_{3\times3} & 0_{3\times1} \\ -c_1\mathbf{I}_{3\times3} & -c_2\mathbf{I}_{3\times3} & -c_3\mathbf{I}_{3\times3} & 0_{3\times1} \\ 0_{1\times3} & 0_{1\times3} & 0_{1\times3} & -c_h \end{bmatrix},$$
$$\mathbf{B} = \begin{bmatrix} 0_{3\times3} & 0_{3\times2} & 0_{3\times2} & 0_{3\times1} & 0_{3\times1} \\ \mathbf{I}_{3\times3}/m & 0_{3\times2} & 0_{3\times2} & 0_{3\times1} & 0_{3\times1} \\ \mathbf{L}_{d1}/m & \bar{\mathbf{J}}_p\mathbf{B}_{d2} & 0_{3\times2} & \bar{\mathbf{J}}_h & 0_{3\times1} \\ 0_{1\times3} & 0_{1\times2} & 0_{1\times2} & 1 & 0 \end{bmatrix}, \quad (65)$$

such that $\bar{\mathbf{J}}_p = \mathbf{J}_p(\mathbf{e}_{p,o}, e_{h,o})$ and $\bar{\mathbf{J}}_h = \mathbf{J}_h(\mathbf{e}_{p,o}, e_{h,o})$. Since the matrix defined in Eq. 64 is a block diagonal matrix, then, the eigenvalues of this matrix are the eigenvalues of the matrices $\mathbf{A}$ and $-\mathbf{L}_d$. As mentioned in section 3.1, the matrix $-\mathbf{L}_d$ is designed to be a negative definite diagonal matrix. In addition, the eigenvalues of the matrix $\mathbf{A}$ are the roots of the polynomial $p(s) = (s+c_h)(s^3+c_3s^2+c_2s+c_1)^3$ which is Hurwitz as implied in subsections 3.1 and 3.2. Thus, the linearized composite error dynamics of the whole system are locally stable on the sliding surface. Notice that the eigenvalues of the linearized composite error dynamics

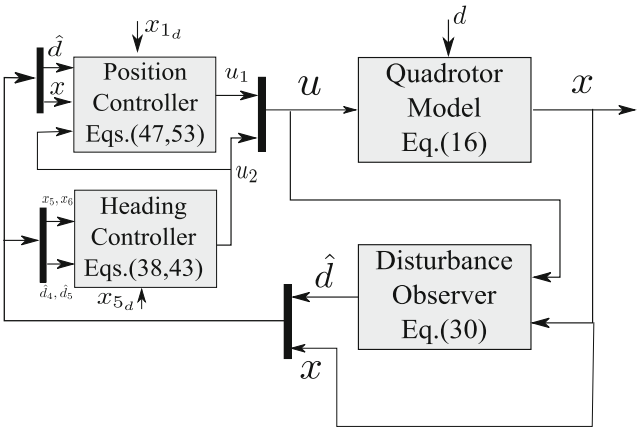

Fig. 2 A block diagram of the developed controller

are independent of the point $(\mathbf{e}_{p,o}, e_{h,o})$ as long as Eq. 63 is linearized around $\mathbf{e}_{d,o} = \mathbf{0}_{9\times1}$. A block diagram showing the structure of the composite controller is found in Fig. 2.

It is worth mentioning that the sliding mode controller completely cancels the effect of the matched disturbance estimation errors on both; the sliding surface dynamics by choosing the gains k_{hs} and k_{ps} as in Eqs. 45, 62 and the reduced model dynamics since these disturbances don't appear in Eqs. 46, 63. This is the main advantage of the controller developed in this work over the the controller developed in [16] in which matched disturbance estimation errors affect the closed loop dynamics. Moreover, the sliding mode controller cancels the effect of the mismatched disturbance estimation errors on the sliding surface dynamics. In addition, by appropriately tuning the coefficients of the reduced-order model, the effect of the mismatched disturbance estimation errors on the reduced-order model dynamics can be attenuated.

4 Simulation Results

The developed composite hierarchical anti-disturbance controller is implemented in simulation and applied to the quadrotor model. The simulation results are presented in this section.

The quadrotor's model parameters used in the test scenario developed in this work are chosen to be $m = 2Kg$, $g = 9.81m/s^2$, $I_x = 41.3g.m^2$, $I_y = 42.2g.m^2$, $I_z = 75.9g.m^2$, $b = 2.551 \times 10^{-5}Ns^2$, $l_a = 0.2m$ and $d = 0.64 \times 10^{-6}Nms^2$. The quadrotor is required to reach the desired position $(x_d, y_d, z_d) = (0, 0, 10)$ with a yaw angle $\psi_d = 0$. The initial conditions of the quadrotor's states are chosen as follows: $x = y = 1m$, $z = 11m$, $\dot{x} = \dot{y} = \dot{z} = 0.1m/s$, $\phi = \theta = \psi = 2deg$, $p = q = r = 0.1rad/s$, $U_1 = 19.62\ N$ and $\dot{U}_1 = 0N/s$. The sliding mode controller gains are chosen to be $c_h = 40$, $k_h = 2$, $k_{hs} = 5$, $c_1 = 8$, $c_2 = 12$, $c_3 = 6$, $k_p = 5$ and $k_{ps} = 80$. The gains of the disturbance observer are selected as follows, $l_{d1} = l_{d2} = l_{d4} = 1$ and $l_{d3} = l_{d5} = 10$.

In the developed test scenario, wind influences the quadrotor based on the wind model mentioned in Section 2.3. The drag force parameters are chosen as $\rho = 1.2kg/m^3$, $C_{dx} = C_{dy} = 0.3$, $C_{dz} = 0.5$, $A_u = A_v = 0.1m^2$ and $A_w = 0.2m^2$. Two discrete wind gusts are applied. The first discrete wind gust parameters are chosen as $t_1 = 20s$, $t_2 = 40s$, $v_{z1} = -2m/s$, $v_{z2} = -4m/s$, $v_{x1} = v_{y1} = -6m/s$ and $v_{x2} = v_{y2} = -12m/s$. Whereas the second discrete wind gust parameters are selected to be $t_1 = 60s$, $t_2 = 80s$, $v_{x1} = v_{y1} = -12m/s$, $v_{x2} = v_{y2} = -6m/s$, $v_{z1} = -4m/s$ and $v_{z2} = -2m/s$. The parameter W_{20} of the Von-Karman wind turbulence model is chosen to be $W_{20} = 15m/s$. Moreover, a partial actuator failure exists at $t = 50s$ in which the front rotor is assumed to lose 5% of its effectiveness (i.e. $\lambda = 0.95$). To avoid the control

Fig. 3 Drag force disturbances

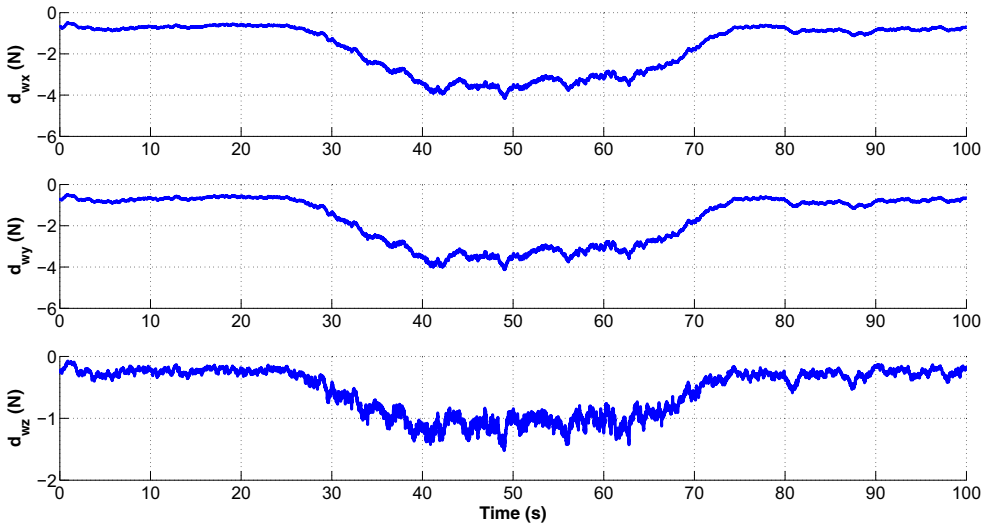

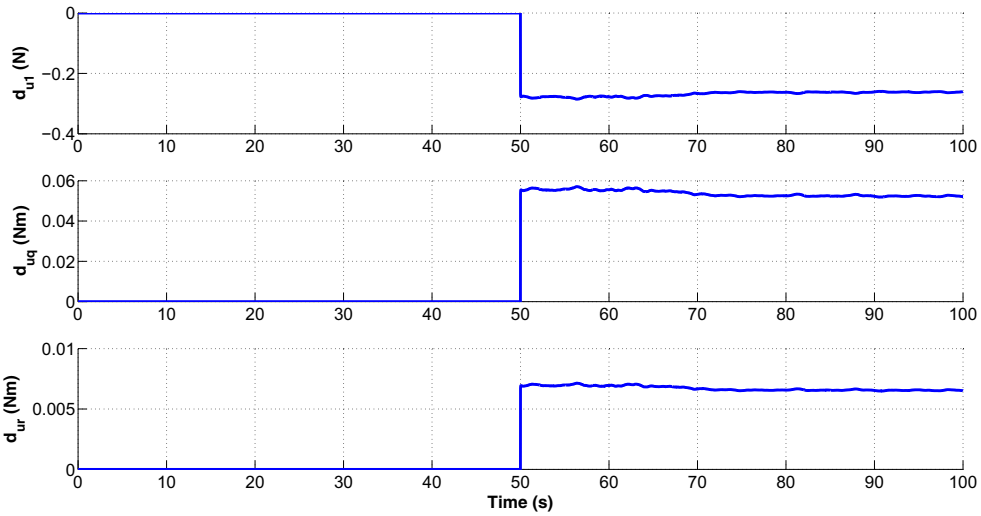

Fig. 4 Partial front rotor failure disturbances

input chattering [1], the sign function is replaced by the saturation function in the control laws in Eqs. 43 and 53. It is proven in simulations that the chattering is attenuated using the saturation function maintaining the quadrotor response almost the same as that using the sign function. Using the saturation function, the dag forces affecting the quadrotor along the inertial axes are shown in Fig. 3 and the forces and torques applied by the actuator failure are shown in Fig. 4. The torque $d_{up} = \bar{U}_2 - U_2$ is not shown because it is equal to zero since the control input U_2 is not affected when the front rotor fails.

In Figs. 5–7, the quadrotor response is shown comparing three controllers; the sliding mode controller (SMC) without the disturbance observer, the composite hierarchical anti-disturbance controller using the sign function (CHADC sign) and the composite hierarchical anti-disturbance controller using the saturation function (CHADC sat). As shown in Fig. 5, lower position error is achieved in the presence of the disturbance observer especially when the mean wind velocity increases in the middle part of the simulation. The response is almost the same in the case of the sign and saturation functions. This can be proven quantitatively using the maximum tracking error norm of the position at steady state which is found to be 2.0294 in the case of the sliding mode control without a disturbance observer, 0.1892 in the case of the disturbance observer-based sliding mode control with the sign function and 0.1955 in the case of the disturbance observer-based sliding mode control with the sat function. As shown in Fig. 6, the euler angles are almost the same in the three cases. Notice that the roll and pitch angles vary within the range of normal operation. The yaw angle does not differ a lot when using the three controller since the disturbances affecting this degree-of-freedom are relatively small. As shown in Fig. 7, chattering is attenuated when using the saturation function. Conversely, chattering occurs in the control inputs U_2, U_3 and U_4 when using the sign function. Notice that the thrust force U_1 is chatter-free using the sign function since the control signal computed

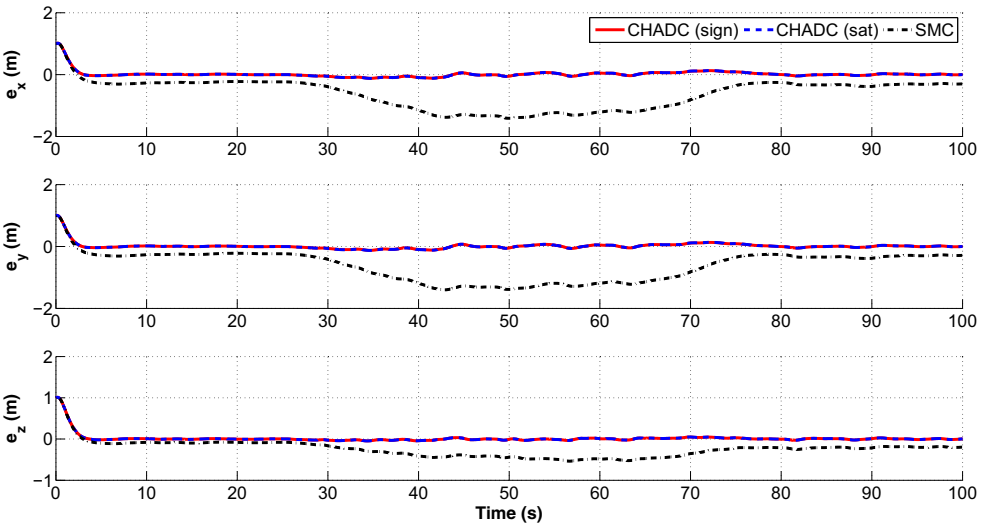

Fig. 5 Quadrotor position error

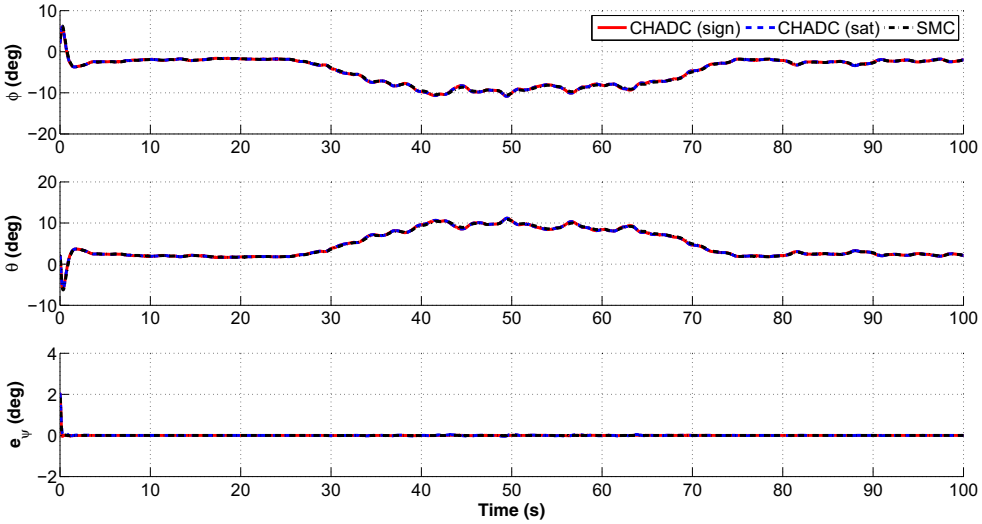

Fig. 6 Quadrotor roll ϕ and pitch θ angles and heading error e_ψ

using the develped controller is the second derivative of the thrust force $\ddot{U}$. By integrating this signal twice, chattering is significantly attenuated.

The disturbance observer estimation errors are shown in Figs. 8–10 where Fig. 8 shows the disturbing force estimation errors, Fig. 9 shows the estimation errors of the disturbances affecting the quadrotor angular velocity, and Fig. 10 shows the disturbing moment estimation errors. In Fig. 8, the estimation errors start increasing at $t = 30s$ due to the increase of the mean wind velocity during the first wind gust. The errors decrease again starting from $t = 70$ since the mean wind velocity decreases during the second wind gust. Although the estimation errors in Figs. 9–10 are very small compared to the estimation errors in Fig. 8, their effects are amplified. This amplification occurs because, while choosing k_{ps} in Eq. 62, these errors, which appear inside $\mathbf{e}_{ph}$, are multiplied by the maximal thrust force U_{1+}. As shown in Fig. 10, the estimation errors e_{dq} and e_{dr} are non-zero at $t = 50s$ because the partial actuator failure takes place at this instant. The estimation error e_{dp} is not affected because the control input U_2 is decoupled from the other control inputs when the front rotor partially fails. The error e_{dp} occurring in the beginning is due to the ignored nonlinear rotational dynamics.

Finally, the composite hierarchical anti-disturbance controller (CHADC) developed in this work is compared to the disturbance observer-based feedback linearization controller (DOFL) derived in [16]. In this test scenario, the quadrotor parameters and the desired position and heading remain the same. The initial conditions are chosen to be all zeros except the quadrotor altitude which is chosen be $z = 10m$. The CHADC gains remain the same. The DOFL controller gains are chosen in such a way that the eigenvalues of the quadrotor closed loop dynamics are all located at $s = -2$. The disturbance observer eigenvalues are located at $s = -1$ in both controllers. To clearly compare both

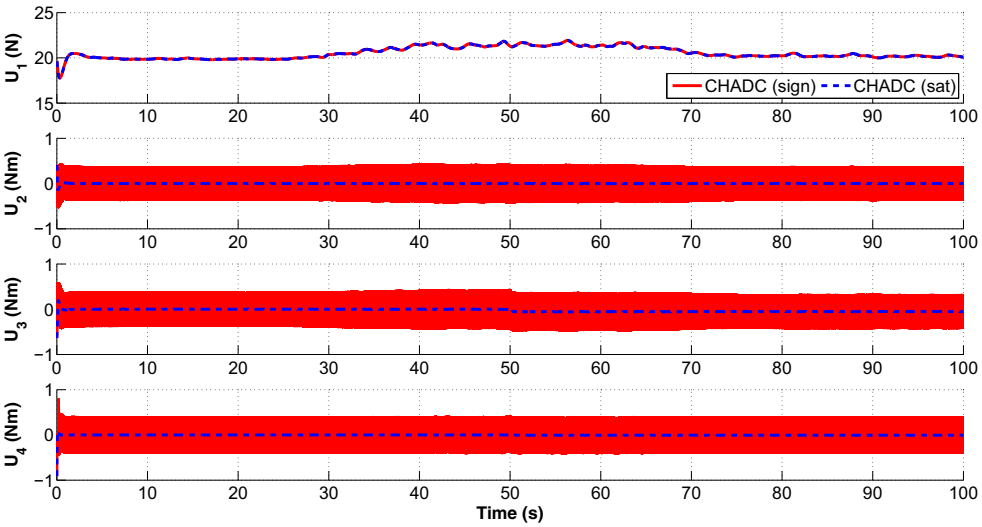

Fig. 7 Quadrotor control inputs

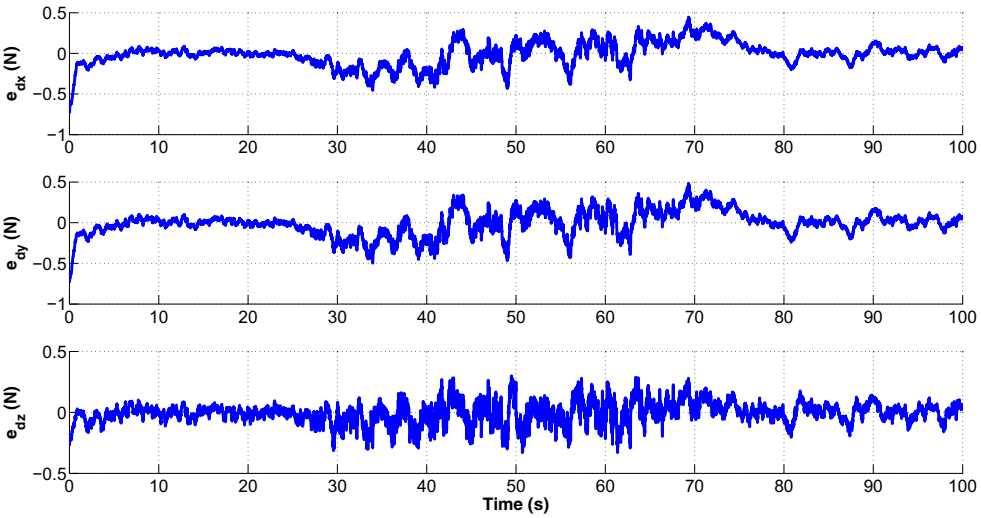

Fig. 8 Disturbance observer estimation error $\mathbf{e}_{d1} = [e_{dx}, e_{dy}, e_{dz}]^\top$

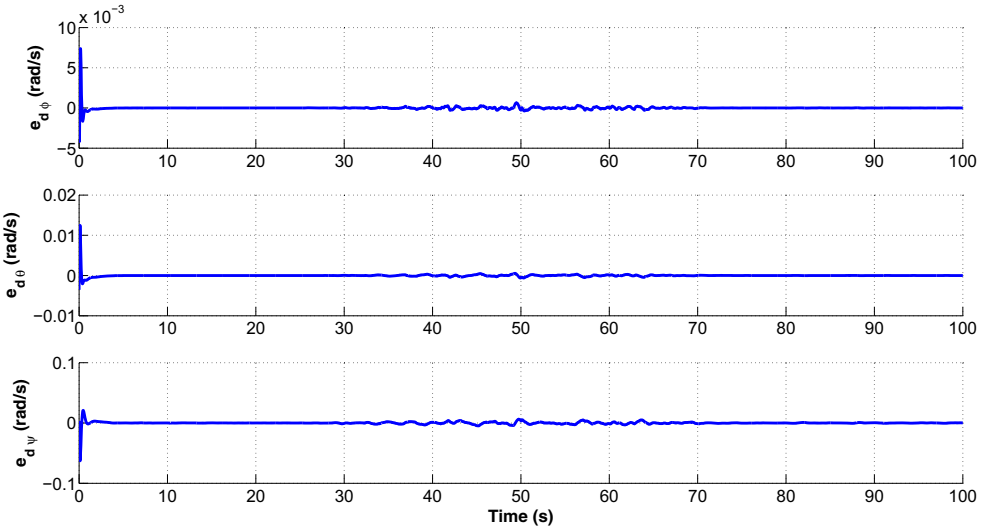

Fig. 9 Disturbance observer estimation error $\mathbf{e}_{d2} = [e_{d\phi}, e_{d\theta}]^\top$ and $e_{d4} = e_{d\psi}$

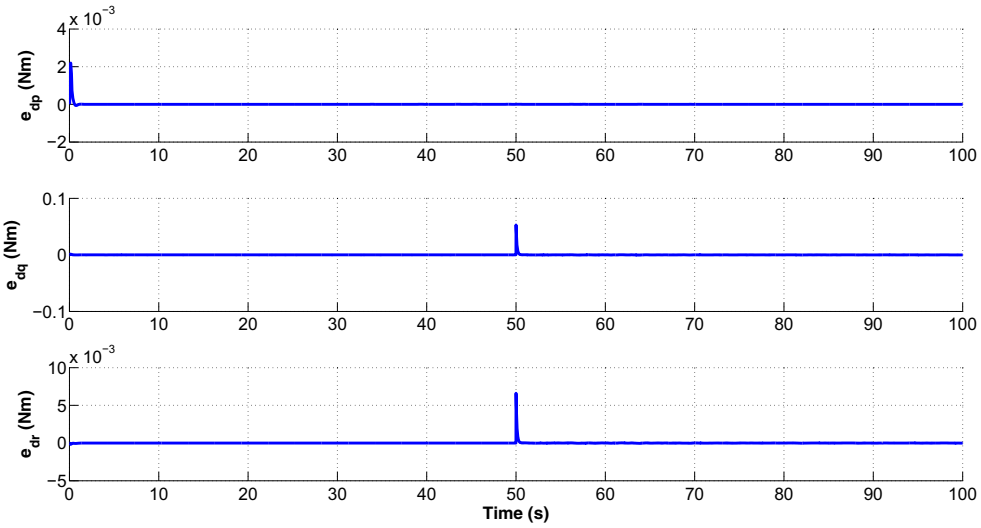

Fig. 10 Disturbance observer estimation error $\mathbf{e}_{d3} = [e_{dp}, e_{dq}]^\top$ and $e_{d5} = e_{dr}$

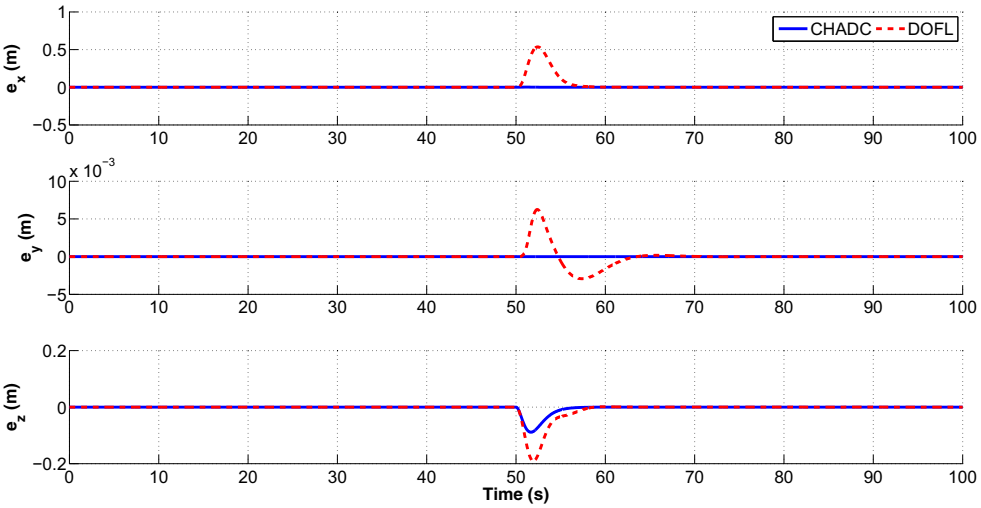

Fig. 11 Quadrotor position error in the presence of 10% front rotor failure in the case of DOFL and CHADC

controllers, the drag force disturbances are disabled and a 10% partial actuator failure of the front rotor is applied solely at $t = 50$. In this case, the partial actuator failure force d_{u1} is considered to be a mismatched disturbance. Whereas, the partial actuator failure moments d_{up}, d_{uq} and d_{ur} are considered to be the matched disturbances. Recall that the disturbance d_{up} is zero because it is not affected by the failure of the front rotor.

Figure 11 shows the quadrotor's position error in both cases. Figure 12 shows the quadrotor's roll and pitch angles as well as the heading error. Figure 13 shows the quadrotor's control inputs. As shown in Fig. 12, the roll and pitch angles in both cases are close to zero. Therefore, by decomposing the actuator failure mismatched disturbing force d_{u1} along the inertial axes, it is found that this mismatched force affects greatly the quadrotor's altitude and has negligible effects on the quadrotor's horizontal position. On the other hand, the quadrotor's horizontal position and heading are affected by the matched disturbing moments d_{uq} and d_{ur} respectively. As shown in Figs. 11 and 12, an overshoot occurs in the position error along the x-axis and in the heading error when the DOFL controller is used. These errors converge to zero after the acturator failure due to the existence of the disturbance observer. No overshoot occurs in the case of CHADC because this controller cancels the effect of matched disturbances completely as mentioned in subsection 3.4. An overshoot occurs in both cases in the position error along the z-axis because the disturbance influencing this degree-of-freedom is mismatched. No overshoot exists in both cases in the position error along the y-axis because the disturbance d_{up} is equal to zero. In Fig. 13, it is shown that the control inputs of both controllers are comparable in magnitude.

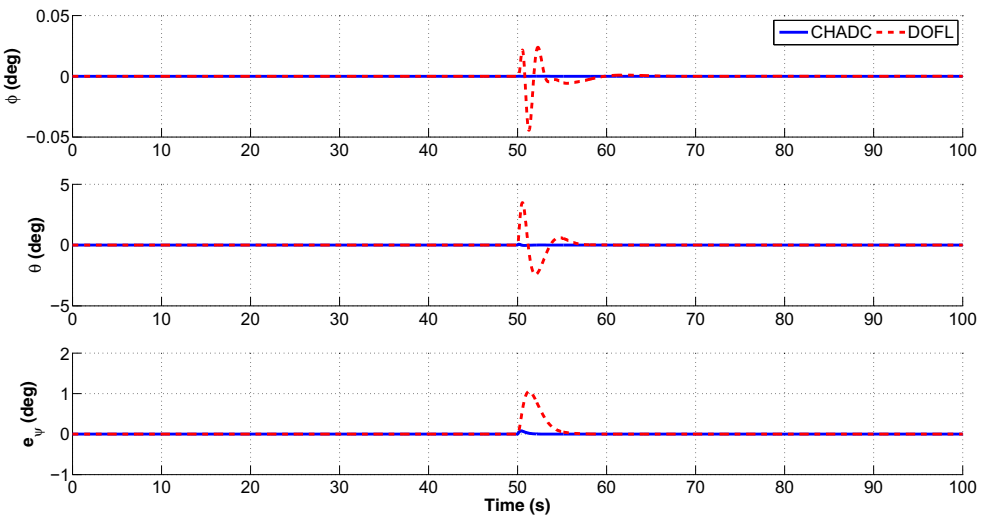

Fig. 12 Quadrotor roll and pitch angles and heading error in the presence of 10% front rotor failure in the case of DOFL and CHADC

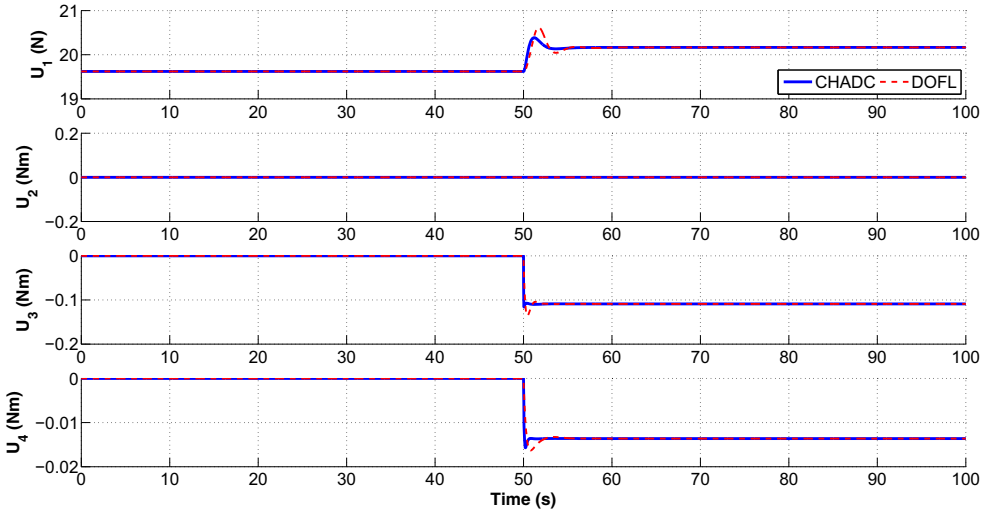

Fig. 13 Quadrotor control inputs in the presence of 10% front rotor failure in the case of DOFL and CHADC

5 Conclusion

In this paper, a composite hierarchical anti-disturbance controller is developed including a disturbance observer, that estimates the constant and slow time-varying disturbances, and a sliding mode controller, that attenuates the fast time-varying disturbances and the disturbance observer estimation errors. Disturbances include disturbing forces and moments as well as neglected nonlinear terms in the rotational dynamics. This simplifies the controller design and leads to the division of the controller into two parts; one for the heading control and the other for the position control. Due to the augmentation of the sliding mode controller with the nonlinear disturbance observer, the disturbances' upper bounds are no longer required. Instead, the upper bounds of the disturbance observer estimation errors are required, which are found to be bounded when the disturbance derivatives and the initial disturbances are bounded and the disturbance observer dynamics are stable. This requirement results in a better performance in terms of the tracking error norm of the quadrotor position at steady state without increasing the sliding mode control gains. Due to the nonlinear quadrotor model, the upper bounds of the quadrotor states and disturbance estimates are also required. The developed controller is tested in simulation by assuming that the front rotor has partially failed in the presence of different types of wind. The simulation results have shown the effectiveness of the proposed controller.

References

1. Khalil, H.K.: Noninear Systems. Prentice-Hall, New Jersey (1996)
2. Bouabdallah, S., Siegwart, R.: Backstepping and sliding-mode techniques applied to an indoor micro quadrotor. In: Proceedings of the 2005 IEEE International Conference on Robotics and Automation, 2005. ICRA 2005, pp. 2247–2252. IEEE (2005)
3. Runcharoon, K., Srichatrapimuk, V.: Sliding mode control of quadrotor. In: 2013 International Conference on Technological Advances in Electrical, Electronics and Computer Engineering (TAEECE), pp. 552–557. IEEE (2013)
4. Xu, R., Özgüner, Ü.: Sliding mode control of a quadrotor helicopter. In: 45th IEEE Conference on Decision and Control, 2006, pp. 4957–4962. IEEE (2006)
5. Bouadi, H., Bouchoucha, M., Tadjine, M.: Sliding mode control based on backstepping approach for an uav type-quadrotor. World Acad. Sci. Eng. Technol. **26**(5), 22–27 (2007)
6. Madani, T., Benallegue, A.: Backstepping sliding mode control applied to a miniature quadrotor flying robot. In: 2006-32nd Annual Conference on IEEE Industrial Electronics, IECON, pp. 700–705. IEEE (2006)
7. Sharifi, F., Mirzaei, M., Gordon, B.W., Zhang, Y.: Fault tolerant control of a quadrotor uav using sliding mode control. In: 2010 Conference on Control and Fault-Tolerant Systems (SysTol), pp. 239–244. IEEE (2010)
8. Waslander, S.L., Hoffmann, G.M., Jang, J.S., Tomlin, C.J.: Multi-agent quadrotor testbed control design: integral sliding mode vs. reinforcement learning. In: 2005 IEEE/RSJ International Conference on Intelligent Robots and Systems, 2005 (IROS 2005), pp. 3712–3717. IEEE (2005)
9. Lee, D., Kim, H.J., Sastry, S.: Feedback linearization vs. adaptive sliding mode control for a quadrotor helicopter. Int. J. Control. Autom. Syst. **7**(3), 419–428 (2009)
10. Islam, S., Faraz, M., Ashour, R.K., Cai, G., Dias, J., Seneviratne, L.: Adaptive sliding mode control design for quadrotor unmanned aerial vehicle. In: 2015 International Conference on Unmanned Aircraft Systems (ICUAS), pp. 34–39. IEEE (2015)
11. Zheng, E.-H., Xiong, J.-J., Luo, J.-L.: Second order sliding mode control for a quadrotor uav. ISA Trans. **53**(4), 1350–1356 (2014)
12. Li, S., Yang, J., Chen, W.-H., Chen, X.: Disturbance Observer Based Control: Methods and Applications. CRC Press, Boca Raton (2014)
13. Guo, L., Cao, S.: Anti-disturbance control theory for systems with multiple disturbances. A survey. ISA transactions **53**(4), 846–849 (2014)
14. Chen, W.-H., Yang, J., Guo, L., Li, S.: Disturbance-observer-based control and related methods—an overview. IEEE Trans. Ind. Electron. **63**(2), 1083–1095 (2016)

15. Hancer, C., Oner, K.T., Sirimoglu, E., Cetinsoy, E., Unel, M.: Robust hovering control of a quad tilt-wing uav. In: IECON 2010-36th Annual Conference on IEEE Industrial Electronics Society, pp. 1615–1620. IEEE (2010)
16. Aboudonia, A., El-Badawy, A., Rashad, R.: Disturbance observer-based feedback linearization control of an unmanned quadrotor helicopter. Journal of Systems and Control Engineering. https://doi.org/10.1177/0959651816656951 (2016)
17. Besnard, L., Shtessel, Y.B., Landrum, B.: Control of a quadrotor vehicle using sliding mode disturbance observer. In: Proceedings of the American Control Conference, pp. 5230–5235. IEEE (2007)
18. Besnard, L., Shtessel, Y.B., Landrum, B.: Quadrotor vehicle control via sliding mode controller diriven by sliding mode disturbance observer. J. Frankl. Inst. **349**(2), 658–684 (2012)
19. Wang, H., Chen, M.: Sliding mode attitude control for a quadrotor micro unmanned aircraft vehicle using disturbance observer. In: Proceedings of the IEEE Chinese Guidance, Navigation and Control Conference, pp. 568–573. IEEE (2014)
20. Ginoya, D., Shendge, P.D., Patre, B.M., Phadke, S.B.: A new state and perturbation observer based sliding mode controller for uncertain systems. Int. J. Dyn. Control. **4**(1), 92–103 (2016)
21. Londhe, P.S., Dhadekar, D.D., Patre, B.M., Waghmare, L.M.: Uncertainty and disturbance estimator based sliding mode control of an autonomous underwater vehicle. International Journal of Dynamics and Control. https://doi.org/10.1007/s40435-016-0260-z (2016)
22. Yang, J., Li, S., Xinghuo, Y.: Sliding-mode control for systems with mismatched uncertainties via a disturbance observer. IEEE Trans. Ind. Electron. **60**(1), 160–169 (2013)
23. Pounds, P., Mahony, R., Corke, P.: Modelling and control of a large quadrotor robot. Control Eng. Pract. **18**(7), 691–699 (2010)
24. Mahony, R., Kumar, V., Corke, P.: Multirotor aerial vehicles: Modeling, estimation, and control of quadrotor. IEEE Robot. Autom. Mag. **19**(3), 20–32 (2012)
25. Castaldi, P., Mimmo, N., Naldi, R., Marconi, L.: Robust trajectory tracking for underactuated vtol aerial vehicles: Extended for adaptive disturbance compensation. In: Proceedings of 19th IFAC World Congress, vol. 19, pp. 3184–3189 (2014)
26. Hoblit, F.M.: Gust Loads on Aircraft: Concepts and Applications. Aiaa (1988)
27. Isidori, A.: Nonlinear Control Systems. Springer Science & Business Media, Berlin (2013)

Ahmed Aboudonia received his B.Sc. and M.Sc. in Mechatronics Engineering from the German University in Cairo (GUC), Cairo, Egypt. He worked as a teaching assistant in the Mechatronics department in the GUC for one year. He is currently a master student in the control engineering program in Sapienza University in Rome, Italy. His research interests include optimal and robust control.

Ramy Rashad received his B.S. (2013) and M.S. (2015) in Mechatronics Engineering from the German Univ. in Cairo (GUC) in Egypt. He joined the mechatronics engineering department in the GUC as a teachign assistant from 2013-2016. He is currently a Ph.D. candidate in the robotics and mechatronics group in the Univ. of Twente, Netherlands. His research interests are aerial robotics, nonlinear and geometric control, and port-Hamiltonian dynamic systems.

Prof. Dr. Ayman A. El-Badawy was born in Cairo, Egypt on August 17, 1972. He received a B.Sc. and M.Sc. degrees in Mechanical Engineering in 1993 and 1995 from the American University in Cairo. He received his Ph.D. in Mechanical Engineering in 2000 from Virginia Polytechnic Institute and State University. He has industrial experience with A.O. Smith Corporation, USA and Nile Aster, Egypt. He is currently the head of mechatronics engineering department at the German University in Cairo.